ARL-TR-9157 ● Mar 2021

DEVCOM ARMY RESEARCH LABORATORY

Characterization of Additively Manufactured Silicon Carbide (SiC)-Based Nanocomposites for Body Armor Applications

by Tyrone L Jones, Jerry LaSalvia, Nicholas Ku, Kristopher Behler, Douglas Harris, Bill Goodman, Shawn Kelso, Brenden M Minei, and Mehrdad N Ghasemi Nejhad

NOTICES

Disclaimers

The findings in this report are not to be construed as an official Department of the Army position unless so designated by other authorized documents.

Citation of manufacturer's or trade names does not constitute an official endorsement or approval of the use thereof.

Destroy this report when it is no longer needed. Do not return it to the originator.

ARL-TR-9157 ● Mar 2021

Characterization of Additively Manufactured Silicon Carbide (SiC)-Based Nanocomposites for Body Armor Applications

Tyrone L Jones, Jerry LaSalvia, Nicholas Ku, Kristopher Behler, and Douglas Harris
Weapons and Materials Research Directorate,
DEVCOM Army Research Laboratory

Bill Goodman and Shawn Kelso
Goodman Technologies

Brenden M Minei and Mehrdad N Ghasemi Nejhad
Hawai'i Nanotechnology Labs, Department of Mechanical Engineering,
University of Hawai'i at Manoa

REPORT DOCUMENTATION PAGE

Form Approved
OMB No. 0704-0188

1. REPORT DATE *(DD-MM-YYYY)*	2. REPORT TYPE	3. DATES COVERED (From - To)
March 2021	Technical Report	November 2019–January 2021

4. TITLE AND SUBTITLE
Characterization of Additively Manufactured Silicon Carbide (SiC)-Based Nanocomposites for Body Armor Applications

5a. CONTRACT NUMBER

5b. GRANT NUMBER

5c. PROGRAM ELEMENT NUMBER

6. AUTHOR(S)
Tyrone L Jones, Jerry LaSalvia, Nicholas Ku, Kristopher Behler, Douglas Harris, Bill Goodman, Shawn Kelso, Brenden M Minei, and Mehrdad N Ghasemi Nejhad

5d. PROJECT NUMBER

5e. TASK NUMBER

5f. WORK UNIT NUMBER

7. PERFORMING ORGANIZATION NAME(S) AND ADDRESS(ES)
DEVCOM Army Research Laboratory
ATTN: FCDD-RLW-PE
Aberdeen Proving Ground, MD 21005

8. PERFORMING ORGANIZATION REPORT NUMBER
ARL-TR-9157

9. SPONSORING/MONITORING AGENCY NAME(S) AND ADDRESS(ES)

10. SPONSOR/MONITOR'S ACRONYM(S)

11. SPONSOR/MONITOR'S REPORT NUMBER(S)

12. DISTRIBUTION/AVAILABILITY STATEMENT
Approved for public release; distribution is unlimited

13. SUPPLEMENTARY NOTES

14. ABSTRACT
A team of researchers from the US Army, Goodman Technologies Small Business, and the University of Hawai'i evaluated the mechanical properties and ballistic integrity of additively manufactured ceramic armor plates fabricated using a novel additive-manufacturing method. The method involved a proprietary compaction molded (Z-process) on nanopastes and subsequent ceramization in a sealed inert high-temperature furnace using five cycles of polymer infiltration and pyrolysis. The processed ceramic formulations concluded from a design of experiments had a composition of SiC-Si-B6O-BN-SiC whiskers–SMP-10 nanopaste. Plates (90 × 90 × 8 mm) were produced for ballistic analysis in accordance with established procedures, using a 50.8-mm-thick aluminum 6061 plate as backing and witness plates in the case of penetration or deformation. Six silicon carbide (SiC)-based nanocomposite plates were examined ballistically (one shot per plate) against the 12.7-mm APM2 projectile at an impact velocity of 848 m/s. Variants of cracks, discovered during investigation of the material, were the result of the thermal mismatch of the blended material. Consequently, these mechanisms in these materials yielded lower coefficients of ceramic performance during penetration-resistance studies.

15. SUBJECT TERMS
additive manufactured, compaction molded, silicon carbide, ceramic performance, depth of penetration

16. SECURITY CLASSIFICATION OF:			17. LIMITATION OF ABSTRACT	18. NUMBER OF PAGES	19a. NAME OF RESPONSIBLE PERSON
a. REPORT	b. ABSTRACT	c. THIS PAGE			Tyrone Jones
Unclassified	Unclassified	Unclassified	UU	29	19b. TELEPHONE NUMBER (Include area code) (410) 278-6223

Contents

List of Figures

List of Tables

Acknowledgments

The authors would like to acknowledge Clifford Hubbard and William Gamble for their technical expertise and assistance. The authors would also like to acknowledge technicians Donnie Little and Perry Peregino for their ballistic assistance.

1. Introduction

1.1 Filling a Critical Need of the Army Advanced Manufacturing Initiative (AAMI)

On October 4, 2019, Secretary of the Army Ryan D. McCarthy approved Army Directive 2019-29, "Enabling Readiness and Modernization through Advanced Manufacturing," for the purpose of achieving a competitive edge against near-peer adversaries.[1] This directive, also called the AAMI,[2] is in accordance with the Presidential Executive Order 13329 (69 FR 9181), "Encouraging Innovation in Manufacturing".[3]

1.2 Three Core Principles of the AAMI

The AAMI has three core principles with regard to strategy. First, the Army must develop a holistic, threat-based strategy for the investment in and use of advanced methods and materials. Executing the strategy will require partnership from the private sector. As such, the policy allows for incentives designed to promote industry investment in advanced technologies. Second, the Army will incorporate advanced manufacturing upfront and throughout a system's lifecycle. And third, when using advanced manufacturing, the Army needs to be mindful of intellectual-property implications and return on investment.

1.3 Benefits of Advanced Manufacturing

It is believed advanced manufacturing will provide the Army with benefits not currently available through conventional manufacturing practices.[1–3] These are thought to include 1) increased system performance through lighter and stronger materials, 2) part designs not limited by conventional manufacturing methods, 3) reduction of potential failure points in complex components by producing them in a single step, 4) reduction of component development time by rapidly producing prototype components for evaluation, 5) reduction of the need for stockpiling parts or reliance on supply chain, and 6) the as-needed ability to fabricate closer to the point of need.

The work conducted during the Phase I and II projects by the US Army Combat Capabilities Development Command (DEVCOM) Army Research Laboratory (ARL) and Goodman Technologies (GT) has retroactively addressed the AAMI policy. The armor technology that was developed, GT RoboArmor, fills an Army Critical Gap need by the additive manufacturing of lightweight silicon carbide (SiC) ceramic matrix nanocomposites armor in form of fitting shapes, and at the

point of need. This is a capability that does not presently exist in industry. "Advanced manufacturing enhances the supply chain and sustainment efforts, both forward in the field and in our maintenance depots, enabling Soldiers to quickly manufacture critical parts and supplies at the point of need," said Gen. Gus Perna, commanding general of the U.S. Army Materiel Command.[1]

2. Experimental Methodologies

2.1 Material Methodologies

These studies explored nanopastes and considered the materials SiC, B_4C (boron carbide), BN (boron nitride), and B_6O (boron suboxide); the sizes of particles (microscopic and nanoparticles); and firing temperatures (1000 °C and 1400 °C) invoked by two drastically different heating methods. The developed SiC-based nanocomposite panels were tested employing the ASTM C 1161-02C standard with the dimensions of thickness = 3 mm, width = 4 mm, and length = 45 mm^4 to evaluate the materials' strength, stiffness, and toughness. All mechanical-properties characterization of the material was conducted on the manufactured plates employing the proprietary Z-process method developed with the GT team and the University of Hawai'i. The GT team's design of experiments (DOE) listed five experiments to be conducted initially, and in sequence, to elucidate the DOE main parameters and dependencies (intrinsic or extrinsic) and to make the DOE studies focused and efficient; that is, reducing the size of the circle around the optimum solutions, hence reaching the optimum solution faster, more manageably, and with lower costs.

Sample densities were determined using the Archimedes' principle. Sample composition was determined using a Bruker D8 Discover (Billerica, Massachusetts) X-ray diffractometer. The plate was also machined and polished to expose cross sections that were perpendicular as well as parallel to the compaction-molded (Z-process) axis. The microstructure of the plates was then determined by optical and scanning electron microscopy imaging of the cross sections. Chemistries were investigated using energy dispersive X-ray spectroscopy (EDS).

2.2 Terminal Ballistic Impact Methodologies

Depth of penetration (DOP) experiments were designed to determine the relative ballistic performance of different ceramic materials while minimizing the influence of target configuration.[5] For DOP testing, a projectile is fired into a ceramic tile adhesively bonded to a thick metal backer plate such that the projectile will not deform the back surface of the metal plate. These experiments avoid the

fundamental problem of V_{50} ballistic dependence on armor design (e.g., front-to-back plate ratio and material), require fewer shots than V_{50} tests, and have a sensitivity equivalent to that of other ballistic test methods.[6] Differences in penetration depth into the metal plates provides a comparison by which to rank the performance of the ceramic materials.

The target configuration used for these experiments is illustrated in Fig. 1. The target consisted of a 90- × 90-mm ceramic tile at a thickness of 8 mm, backed up by two plates of aluminum alloy 6061 (AA6061)[7] of 50.8-mm (2-inch) thickness. An epoxy resin, Dureflex Optical Aliphatic Polyether Polyurethane Grade A4700, was used to attach each tile to the first 50.8-mm plate. AA6061 was chosen as a well-characterized and readily available backer material. The aluminum backer plates were also expected to provide better resolution than steel plates. No cover plate was employed.

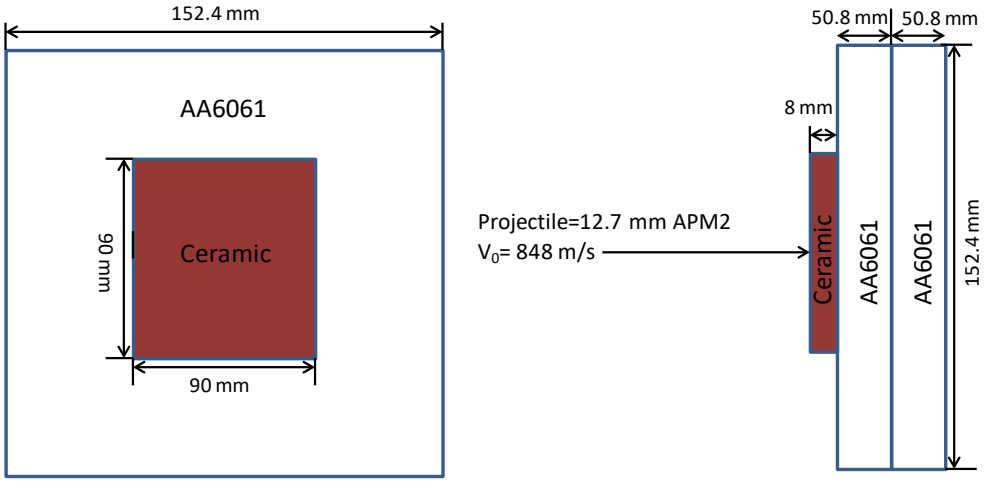

Fig. 1 Ceramic DOP target assembly

All ballistic impact experiments were conducted at the DEVCOM Army Research Laboratory with the sample size n=6 per ceramic composite. The test projectile included a hardened steel-core penetrator with length of 47.6 mm (1.875 inch), a diameter of 10.87 mm (0.428 inch), and an aspect ratio of 4, and is also known as the 12.7-mm APM2 round (Fig. 2). The nominal projectile weight was 46 g, and core density was 7.85 g/cc.

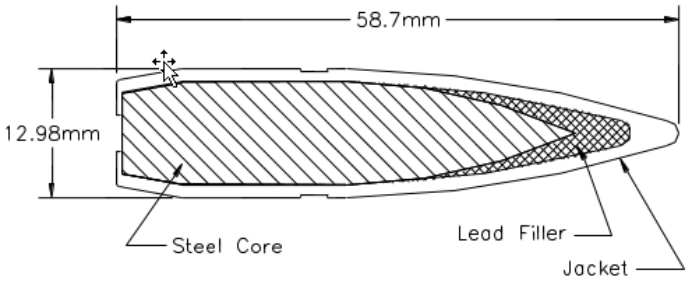

Fig. 2 Cross section of a 12.7-mm APM2

The impact velocity used for all experiments was nominally 848 m/s (2782 ft/s), although some shots were varied from 824 m/s (2704 ft/s) up to 872 m/s (2861 ft/s) into the aluminum back plates alone to provide for DOP corrections for velocity variations. The velocity was chosen in order to produce a range of practical residual penetrations while being consistent with normal operating conditions.

Projectiles with 3° or greater of total yaw were excluded from analysis; previous studies had indicated this as an appropriate cutoff point for ballistic tests at zero obliquity. Measurement of the projectile yaw and velocity was accomplished using a Hewlett-Packard 150-kV Flash X-Ray System in two orthogonal planes.

All residual penetration measurements were obtained by sectioning the AA6061 plates. A band saw was used to section all penetration cavities, and measurements were made using Vernier calipers to the deepest portion at the cavity (as indicated in Fig. 3). Measurement of the "a" value avoids errors that could be caused by deformation of the aluminum block around the entrance cavity.

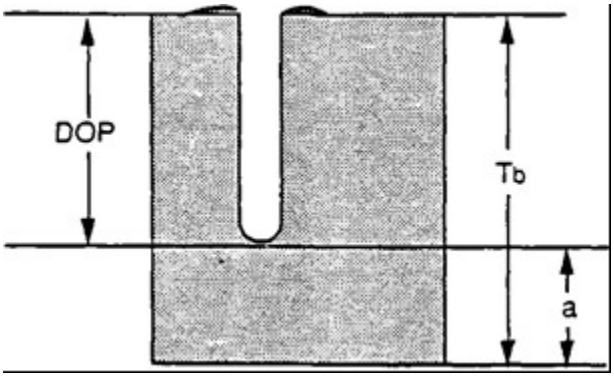

DOP = T_b – a

Fig. 3 Measurement of residual penetration[8]

The contributions of the dynamic failure mechanisms (stiffness and deceleration) attributed to the aluminum tiles, which contributed to the performance of the aluminum plates, were normalized through deconstructing their interference employing a proprietary algorithm.

3. Results and Discussion

3.1 Material Characterization

Across nine plates the density of the material was measured to be 2.370 g/cm^3 with a standard deviation of 0.010 g/cm^3. Based on a theoretical density estimate of 3.014 g/cm^3, the plates are approximately 79% dense. This finding was puzzling since during Archimedes density measurements the balance stabilized very quickly during the suspended-mass measurements. Two possible explanations are the theoretical density estimate is wrong because of the number of phases present and/or because the Z-process involves multiple infiltration steps, it would be natural that internal porosity becomes sealed off from the surface of the plate. In any event, the small standard deviation shows the Z-process results in material that is relatively homogeneous among plates.

The composition of the sample was determined by analyzing the X-ray diffraction pattern shown in Fig. 4. Each peak is marked with Miller indices in a color corresponding to the identified phase. Identification was made using the Crystallography Open Database, with the pattern number used for identification listed in the legend. The SiC-3C (β-SiC), SiC-6H (α-SiC), silicon (Si), B_6O, and graphite are present. The most common form of SiC in the samples is SiC-3C. This is the form of SiC that results from pyrolysis and crystallization of a polymer precursor. While BN was added to the constituent paste, no BN is present in the sample plate. While Si was added to react with residual carbon (which is the result of sintering the preceramic polymer) in the sample and aid densification, both Si and graphite are present in the manufactured plate. These phases are generally considered detrimental to ballistic performance.

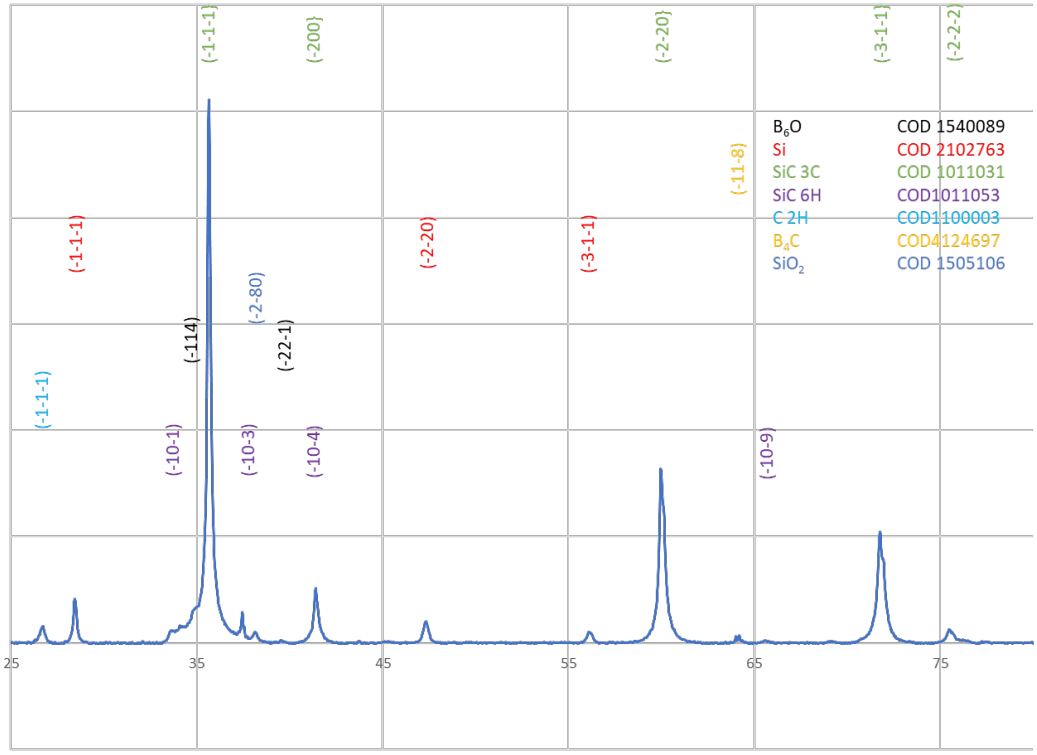

Fig. 4 X-ray diffraction pattern of the sample plate with Miller indices of the identified phases for each peak listed

Figure 5 shows a cut and polished cross section of a manufactured plate. The material in the plate was quite inhomogeneous, which was evident in the varying shades through the sample. This inhomogeneity seemed to correspond to the concentration of SiC whiskers. Significant cracking was visible throughout the microstructure. This would be highly detrimental to any mechanical or armor applications.

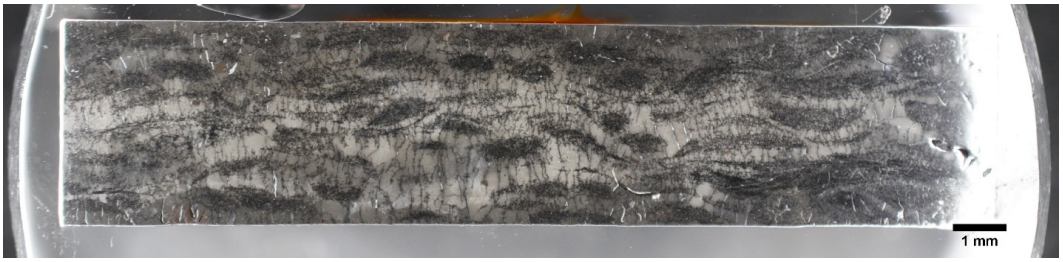

Fig. 5 Optical photograph of polished cross section cut parallel to the Z-direction

In addition to optical imaging, scanning electron microscopy (SEM) imaging was conducted to view the microstructure. Figure 6A shows the tip of a crack that was visible optically in Fig. 5. The size of the crack's opening suggests it is process related, likely from the polymer infiltration and pyrolysis (PIP) process.[9] Polymer-

derived ceramic precursors undergo significant shrinkage during conversion that can cause such fissures in the final ceramic. Figure 6B shows a separate area of the same cross section with many circular cross sections of SiC whiskers of about 20 μm in diameter present. There is an increase in concentration of whiskers from area to area due to the mixing and processing. Also visible are many dark-black patches and large (50–60 μm) bright grains, which are identified as graphite and Si, respectively. Both materials are generally believed to be detrimental to armor performance, as they act as crack initiators. Fine cracks, in Fig. 6C, can be seen running around the interfaces among the SiC whiskers and fine-grained matrix material. These cracks are likely due to the coefficient of thermal expansion's mismatch between the materials occurring during the heating and cooling cycles. Figure 6D shows the individual micron-sized grains can be viewed. Figure 6E shows a cross section of the plate taken perpendicular to the Z-direction. The cross section of the SiC whiskers have a much higher aspect ratio when compared with the images in Fig. 6A and 6B. This shows the orientation of the whiskers along this plane. Also visible in this area are large Si grains and agglomerates of graphite.

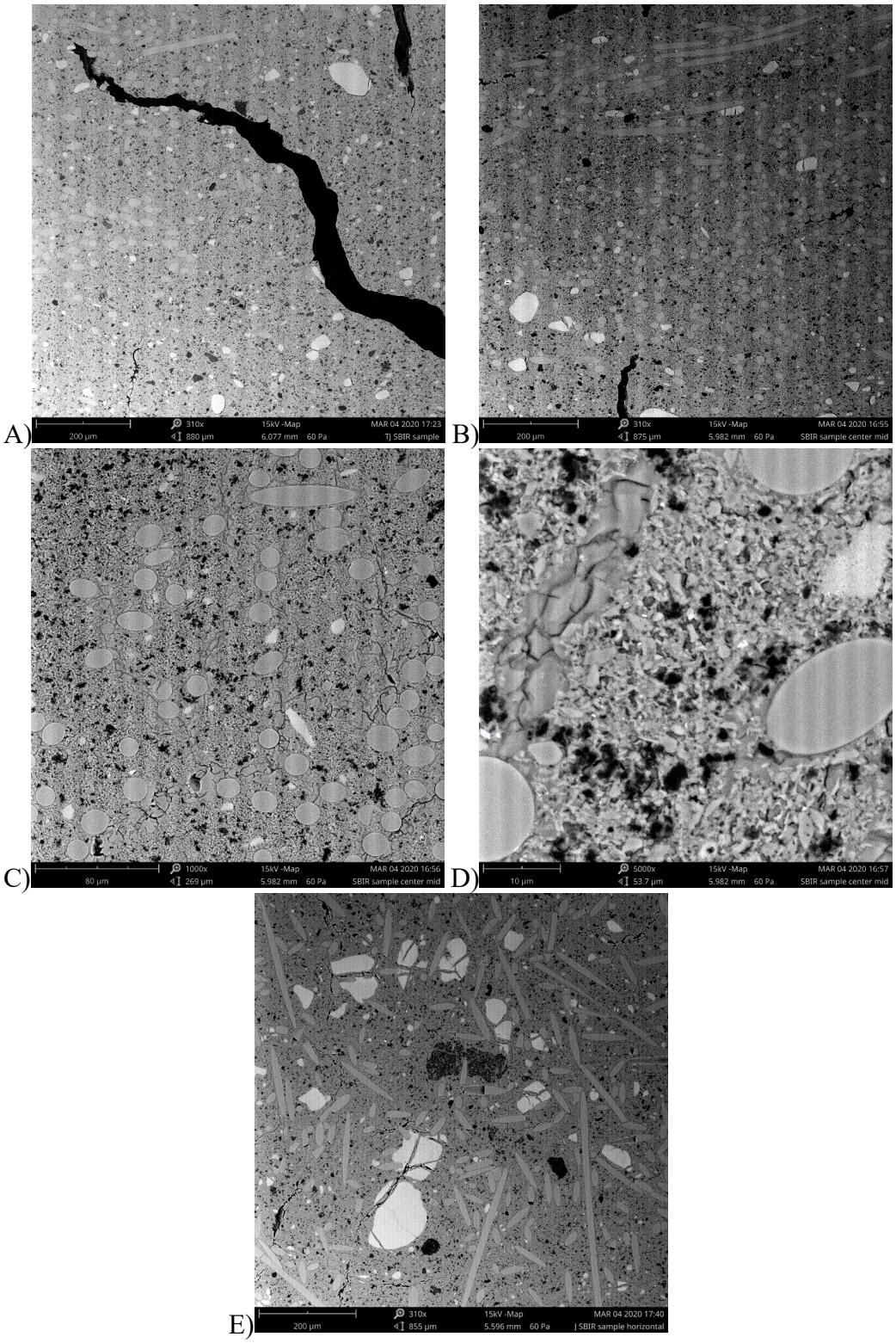

Fig. 6 Microstructural images of the plate material: Image A was taken from a cross section parallel the Z-direction, B–D from same cross section show another area of sample at successively higher magnifications, and E was taken from cross section perpendicular to Z-direction.

Knoop hardness (2 kgf) of the surface and cross section of the material was measured from a 6 × 6 grid of indents with 600-µm spacing in both X and Y directions (Fig. 7). The hardness of the cross-sectioned material was 5.0 ± 1.57 GPa, with a large variability of 2.6 to 7.4 GPa from using 24 data points. The sample surface had a hardness of 6.4 ± 0.78 GPa with a variability from 4.1 to 8.1 GPa. The increase in hardness of the surface may be due to an increase of whiskers aligned parallel to the surface (long aspect ratio of the whisker) leading to an increase in indent interaction with the whiskers. There was no observed excessive spall around the indents.

Data points were removed due to the indent being too asymmetric, >12%, and/or having a second phase at either the crack tips or center of the indent.

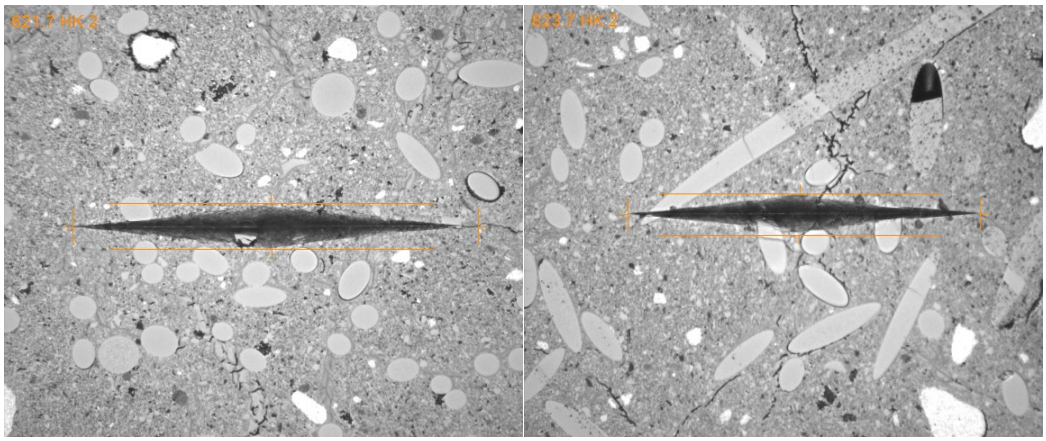

Fig. 7 Optical images of 2-kgf Knoop indents on the cross section (left) and the surface (right) of the samples provided

According to the DOE experiments, coupons were fabricated to perform ASTM C 1161-02C's 4-point bend testing. The data derived from these tests were flexural strength, stiffness, strain to failure, and toughness. The materials evaluated were 1) 100%SiC, 2) 100%B_4C, 3) 50%SiC+50%B_4C, 4) 50%B_4C+50%BN, 5) 80%SiC+20%BN, and 6) 80%SiC+20%B_6O. Pictures of the test setup and coupons are shown in Fig. 8.

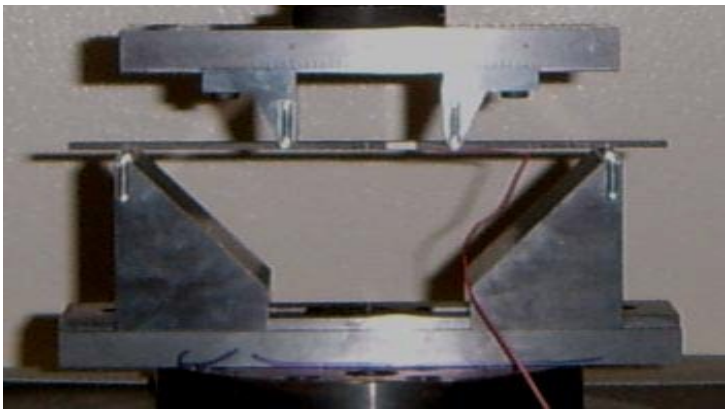

Fig. 8 ASTM C 1161-02C's 4-point bend test measuring flexural strength, stiffness, strain to failure, and toughness

Results of 4-point bend tests are shown in Tables 1 and 2. The best material (based on best-performing samples in terms of the combination of highest strength, stiffness, and toughness) was 100% SiC, followed by 80%SiC+20%BN and then 80%SiC+20%B_6O.

Table 1 Four-point bend test results (ASTM C 1161-02C) for evaluation of flexural strength, stiffness, and toughness (i.e., energy to failure) of SiC-based nanocomposites and PIP conditions

Material	PIP condition (°C)	4-pt. bend strength (MPa)	Bending stiffness (GPa)	Energy to failure (MJ/m^3)
100%SiC	1000	110	91	72
	1400	91	83	53
80%SiC + 20%BN	1000	128	85	100
	1400	78	66	48
80%SiC + 20%B_6O	1000	116	68	111
	1400	71	54	48

The SiC results were compared with those of commercial vendor Poco Graphite. These results are presented in Table 2 and show the Z-process results were in very good agreement.

Table 2 Comparison of strength with SuperSiC[10]

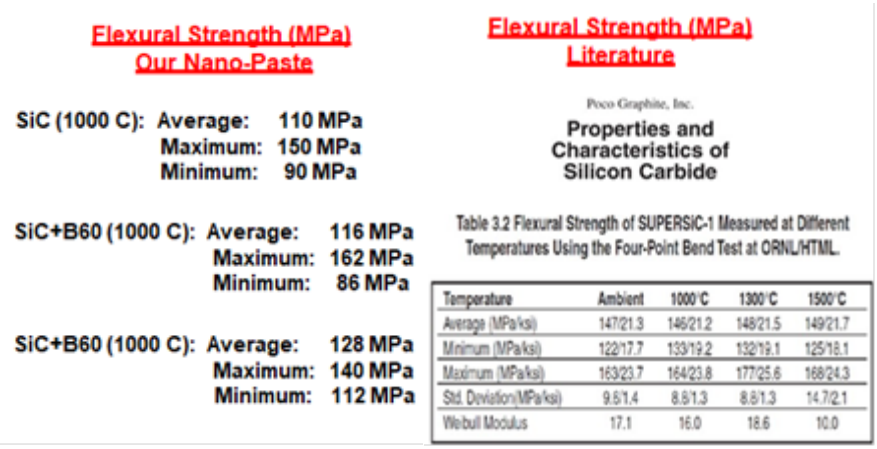

Our next steps were to perform EDS and additional SEM characterizations of the samples. These results are shown in Tables 3–5 for ASTM-standard samples, discs, and polished discs to remove surface oxide. Corresponding SEM images are shown in Figs. 10 and 11. Observation of the SEM images and EDS data revealed that the parts had excess oxygen (particularly at the higher 1400 °C temperature) and also excess carbon. The sources of oxygen for the high-temperature oxidation (particularly at 1400 °C) process was found to be the argon in the vacuum furnace and Shape Memory Polymer (SMP)-10. The excess carbon is also attributed to the SMP-10 polymer. Because of the large quantification uncertainties with light elements like boron (B) by EDS due to low X-ray emission efficiencies and X-ray absorption effects, quantification of "B" was ignored in the EDS analysis and the values of atomic and weight percentages of the elements in Tables 3–5 are calculated based on 100% of Si, carbon (C), and oxygen (O) elements without the consideration of "B", and hence show the relative values of Si, C, and O elements in the samples, which is still very valuable information in combination with the SEM characterizations shown in Figs. 9 and 10.

Table 3 EDS of ASTM-standard, center and surface of samples

Temperature (°C)	Si% (atomic%) [wt%]	C% (atomic%) [wt%]	O% (atomic%) [wt%]
1000 (center and surface similar)	(34.91) [51.70]	(50.51) [31.99]	(13.91) [11.74]
1400 center	(39.06) [57.87]	(48.78) [30.91]	(11.58) [9.77]
1400 surface	(31.49) [46.95]	(29.15) [18.59]	(39.14) [33.25]

Table 4 EDS of disk coupons

Temperature (°C)	Si% (atomic%) [wt%]	C% (atomic%) [wt%]	O% (atomic%) [wt%]
600	(29.79) [48.73]	(62.52) [43.74]	(7.52) [7.00]
1000	(25.05) [40.70]	(45.40) [31.55]	(29.34) [27.16]
1400	(29.94) [44.97]	(24.10) [15.49]	(45.88) [39.26]

Table 5 EDS for polished disks

Temperature (°C)	Si% (atomic%) [wt%]	C% (atomic%) [wt%]	O% (atomic%) [wt%]
1000	(34.86) [53.50]	(49.93) [32.77]	(15.11) [13.21]
1400	(35.57) [53.76]	(45.45) [29.37]	(18.82) [16.20]

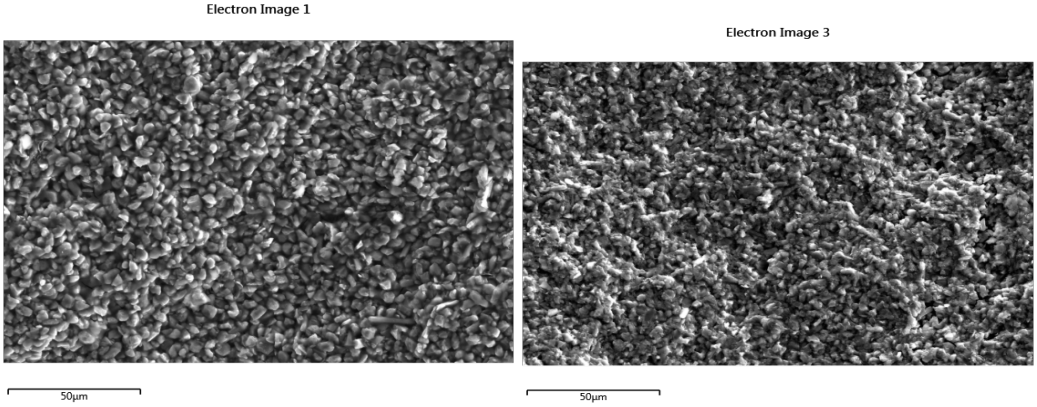

A) 1000 °C ASTM samples B) 1000 °C Disk samples

Fig. 9 Typical SEM of fracture surface

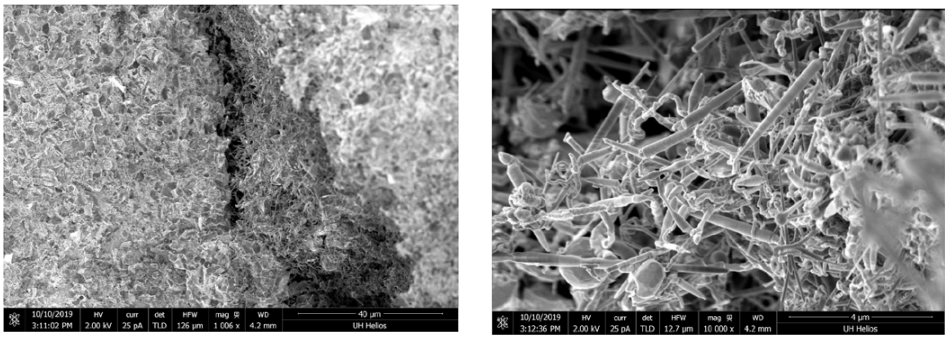

Fig. 10 Typical SEM of ASTM-standard coupon's fracture surface for 1400 °C processing shows SiO_2 needle structures

A decision was made to solve the problem of excess oxygen by using high-purity argon and an oxygen-trap filter for the furnace, along with addition of a small amount of hydrogen to the argon. In addition, to solve the problem of excess carbon it was decided to introduce metallic silicon to the nanopaste. With these suggested process improvements, we combined the three best materials from the DOE to produce SiC-Si-B_6O-BN-SiC whiskers–SMP-10 nanopaste for fabrication of disk and plate coupons for ARL characterization. A set of 38.1- × 6.35-mm ceramic disks were fabricated for measurements of material properties. Additionally, samples of 90- × 90- × 8-mm plates were formulated to perform empirical studies on the penetration resistance of the materials. These coupons are shown in Fig. 11.

Fig. 11 Z-process hybrid armor plates

3.2 Terminal Ballistic Impact Characterization

Six targets comprising SiC-based tiles were ballistically evaluated in accordance with experimental procedures reported in ARL-TR-7768.[8] Each target was fully supported in the test rig by two C-clamps fixed on opposite sides of the target to two vertical frames, as shown in Fig. 12.

A) Front View B) Side View

Fig. 12 Test setup for SiC-based targets in ballistic investigation

The reference velocity for each target–penetrator interaction was 848 m/s. Post-test, the six targets were sectioned down the center of impact and measured for DOP. The cross sections of the penetrator in the witness plate were forensically analyzed with their corresponding impacted SiC plate (Fig. 13). The DOP of the impacted targets ranged from 51 to 64 mm. Very little deformation of the projectile was optically observed, which implied little dwell occurred at the interface of the penetrator and the SiC-based tiles. Work was done on the targets as observed by the targets' fracture and subsequent comminution during ballistic impact. Much of the target surfaces was powder, which is a common feature of additively manufactured ceramics.[8] Comminution is a dominant mechanism over fragmentation, resulting in a less efficient process in dissipating kinetic energy from a ballistic impact.

Left: Cross section of 12-mm APM2 penetrator Right: SiC tile residual target

Fig. 13 Cross section of 12.7-mm APM2 penetrator in target and SiC tile residual target

Left: Cross section of 12-mm APM2 penetrator Right: SiC tile residual target

Fig. 13 Cross section of 12.7-mm APM2 penetrator in target and SiC tile residual target (continued)

The DOPs were normalized to the performance of the AA6061 witness plate, as shown in Table 6. Finally, the ceramic efficiency, C_p, of each ceramic was calculated against the AA6061 witness plate. Since AA6061 was the reference material used in this study, Eq. 1 was used to provide a C_p of the ceramics compared with the reference material:

$$C_p = (\rho_{AA6061}) \frac{DOP_{Base\_AA6061} - DOP_{Corr\_AA6061}}{AD_{Ceramic}} \quad (1)$$

where

DOP_{Base_AA6061} is the average, expected residual depth of penetration into bare aluminum at 848 m/s. DOP_{Corr_AA6061} is the residual depth of penetration into AA6061 after perforating the ceramic tile, corrected for the variations in striking velocity. The calculated C_p value provides a relative comparison of the ceramic with AA6061 (i.e., a C_p of 5 means the ceramic is 5 times more weight effective than AA6061). Ceramic performance is mapped in Fig. 14. The density of plates versus the normalized DOP into the witness plate was plotted for each SiC-based tile. The minima of each level of ceramic efficiency is shown as slash–dot lines. The ceramic efficiency of traditionally manufactured CoorsTek SiC, measured in

an earlier experiment, is added for parametric analysis.[8] While the density of the Z-processed SiC-based tile (2.37 g/cm^3) was lighter than (i.e., 74% of) the density of CoorsTek SiC (3.21 g/cm^3), the ceramic efficiency of Z-processed SiC-based tile was 42% of the CoorsTek SiC (6.94); that is, the Z-processed SiC-based tiles had 58% more penetration depth.

Table 6 DOP for SiC targets

Target shot no.	Depth of penetration (mm)
1	53.49
2	51.49
3	63.91
4	55.47
5	57.05
6	59.69

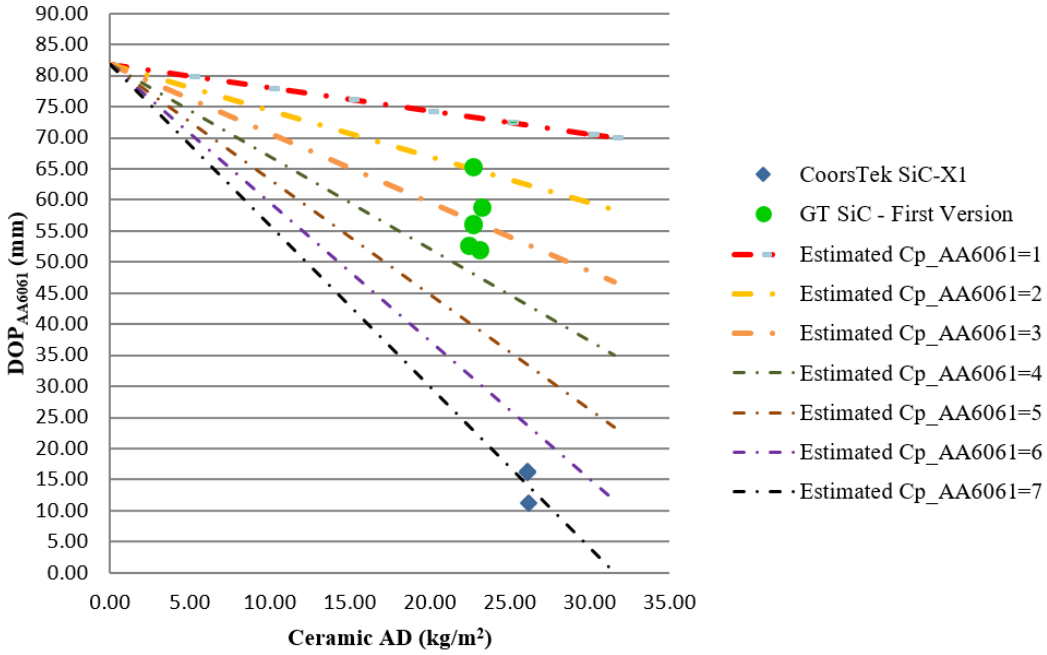

Fig. 14 Ceramic efficiency of SiC-based tiles

4. Conclusion

The manufactured plates consisted of a heterogeneous blend of β-SiC, α-SiC, Si, B_6O, and graphite. BN, one of the constituent material of the printed paste, was not found in the plate and may have reacted during processing (or was not detectable by EDS or X-ray powder diffraction). The microstructure of the material consisted of multiscale features, with large SiC whiskers and Si grains as well as fine, micron-sized SiC grains. Orientation of the whiskers was found to be aligned to the plane perpendicular to the Z-process direction. Extensive multiscale cracking was also found through the sample. Larger fissure-like cracks are inferred to be caused by the volumetric shrinkage expected during the PIP process, with the fine crack around whisker interfaces due to thermal mismatch of the blended material. From a material perspective, the residual Si and graphite phases as well as multiscale cracking can be detrimental to ballistic performance of the plate. In ballistic studies, the 12.7-mm APM2 projectile penetrated the Z-processed SiC-based tiles at 58% more depth than the CoorsTek SiC tiles. One primary reason for the degradation in performance is the lack of work on the nose of the projectile during the target–projectile interaction, potentially due to material's low hardness. The dwell mechanism of the Z-processed and material's compositions needs to be modified and improved, based on the lessons learned from this study, for the future studies. Comminution was the dominant mechanism in the defeat of these projectiles during ballistic impact. Future research will examine the relationship between the multiscale cracks of the Z-processed SiC or other materials and their effects on ceramic armor mechanisms during ballistic impact.

5. References

1. U.S. Army Public Affairs. Secretary of the Army approves new advanced manufacturing policy. 2019 Oct 4. https://www.army.mil/article/228151/secretary_of_the_army_approves_new_advanced_manufacturing_policy.

2. Secretary of the Army. Enabling readiness and modernization through advanced manufacturing. Directive 2019-29. 2019 Sep 18. https://armypubs.army.mil/epubs/DR_pubs/DR_a/pdf/web/ARN19451_AD2019-29_Web_Final.pdf.

3. Executive Office of the President. Encouraging innovation in manufacturing. Executive Order 13329 (69 FR 9179); 2004 Feb 26. https://www.federalregister.gov/documents/2004/02/26/04-4436/encouraging-innovation-in-manufacturing.

4. ASTM C 1161-02C. Standard test method for flexural strength of advanced ceramics at ambient temperature. ATSM International; 2019.

5. Jones TL, Vargas-Gonzalez LR, Scott B, Goodman B, Becker B. Ballistic evaluation and damage characterization of 3-D printed, alumina-based ceramics for light armor applications. J Appl Ceram. 2020 March/April;17(2):424–437.

6. MILSTD-662F. V50 ballistic test for armor. Army Research Laboratory (US); 1997 Dec 17.

7. MIL-DTL-32262. Detail specification: armor plate, aluminum alloy, unweldable applique 6061. Army Research Laboratory (US); 2007 Jul 31.

8. Jones TL, Swab J, Meredith CS, Becker B. The first static and dynamic analysis of 3-D printed sintered ceramics for body armor applications. Army Research Laboratory (US); 2016 Sep. Report No.: ARL-TR-7768.

9. Gudapati VM, Veedu VP, Cao A, Ghasemi Nejhad MN. Experimental investigation of optimal nanoparticle inclusion for enhanced flexural performance in continuous fiber ceramic nanocomposites. J Thermopl Compos Mater. 2009;22(4):421–438.

10. Entegris, Inc. Poco Graphite, SUPERSiC materials data sheet. https://www.entegris.com/content/dam/shared-product-assets/specialty-shared/datasheet-supersic-silicon-carbide-7062.pdf.

List of Symbols, Abbreviations, and Acronyms

AA6061	aluminum alloy 6061
AAMI	Army Advanced Manufacturing Initiative
ARL	Army Research Laboratory
B	boron
B_4C	boron carbide
B_6O	boron suboxide
BN	boron nitride
C	carbon
C_p	coefficient of performance
DEVCOM	US Army Combat Capabilities Development Command
DOP	depth of penetration
EDS	energy dispersive X-ray spectroscopy
GT	Goodman Technologies
O	oxygen
PIP	polymer infiltration and pyrolysis
SEM	scanning electron microscopy
Si	silicon
SiC	silicon carbide
SMP	Shape Memory Polymer

1 (PDF) DEFENSE TECHNICAL INFORMATION CTR DTIC OCA

1 (PDF) DEVCOM ARL FCDD RLD CL TECH LIB

1 (PDF) TEXAS RESEARCH INSTITUTE AUSTIN INC D MOTES

1 (PDF) ZHENG CONSULTING J ZHENG

1 (PDF) SCOTT CONSULTING B SCOTT

1 (PDF) COORSTEK R PALICKA

1 (PDF) KEYENCE M LAMARRE

1 (PDF) SILSBY CONSULTING G SILSBY

1 (PDF) NATIONAL CENTER FOR MANUFACTURING SCIENCES C BOSWELL-KOLLER

1 (PDF) APPLIED RESEARCH LABORATORY, PENNSYLVANIA STATE UNIVERSITY D SWANSON

1 (PDF) HOTEND WORKS B BECKER

1 (PDF) HP WHITE R KINSLER

2 (PDF) CHESAPEAKE TESTING JB JENNINGS J MARTIN

1 (PDF) PEO SOLDIER SFAE SDR SPIE D OTTERSON

1 (PDF) SOCOM HQ FCDD SCS PS M CLARK

1 (PDF) USSOCOM/SOF AT&L-ST C LOVELL

1 (PDF) DEVCOM RDCB DEE K WALLACE

1 (PDF) DEVCOM HQ FCDD CG CT WINS

1 (PDF) DEVCOM AFRC CIE JJ GALLIVAN

1 (PDF) MEDCOM USAMRDC FCMR ZA MJ TALLEY

3 (PDF) NATICK SSC FCDD SCP WI M ROTH RDNS WDE MM MJ HURLEY RDNS SES WI M MAFFEO

30 (PDF) DEVCOM ARL FCDD RLD H MAUPIN FCDD RLC NS G WEAVER FCDD RLW S KARNA A RAWLETT S SCHOENFELD J ZABINSKI FCDD RLW P D HOGGE FCDD RLW PE T JONES FCDD RLW L T SHEPPARD FCDD RLW M B LOVE FCDD RLW B J CAMPBELL L VARGAS-GONZALEZ C HOPPEL FCDD RLW ME K BEHLER D HARRIS N HU J LASALVIA S SILTON

FCDD RLW P
R FRANCART
FCDD RLW PA
S BILYK
FCDD RLW PB
M KLEINBERGER
S SATAPATHY
FCDD RLW PC
D CASEM
J CLAYTON
M FERMEN-COKER
S SEGLETES
FCDD RLW PD
J RUNYEON
FCDD RLW PE
T JONES
P SWOBODA
FCDD RLW PG
N GNIAZDOWSKI